

## Detection of urban effects on precipitation in the Seoul metropolitan area, South Korea

Seong-Ho Hong<sup>a</sup>, Han-Gyul Jin<sup>b</sup>, Jong-Jin Baik<sup>a,\*</sup>

<sup>a</sup> School of Earth and Environmental Sciences, Seoul National University, Seoul 08826, South Korea

<sup>b</sup> Department of Atmospheric Sciences, Pusan National University, Busan 46241, South Korea



### ARTICLE INFO

**Keywords:**

Urban effects  
Precipitation  
Seoul Metropolitan Area  
Rain gauge data  
Downwind precipitation increase

### ABSTRACT

With growing urban population and expanding urban areas, the importance of understanding urban effects on precipitation keeps increasing. This study attempts to detect urban effects on precipitation in the Seoul Metropolitan Area (SMA), South Korea by analyzing hourly rain gauge data during 2005–2020. Precipitation events are categorized according to 850-hPa wind directions, and the precipitation increase from the upwind to downwind regions are examined for different duration and intensity classes of precipitation events. The downwind precipitation increase is largest in summer (39%), especially in August (64%). The August precipitation is analyzed in detail. Precipitation statistically significantly increases in Seoul for weak winds and 25–50 km downwind of the center of Seoul for westerly winds, and the precipitation increases are largest in the afternoon. For the precipitation increases, the increases in frequency and intensity of precipitation events are responsible. Short-duration and heavy precipitation events associated with small-sized precipitation systems initiated within the SMA are mainly responsible for the precipitation increases. The downwind precipitation increase also occurs for southwesterly, southerly, and southeasterly winds, but the increases are associated with large-sized precipitation systems.

### 1. Introduction

Cities affect local and regional precipitation (Shepherd, 2005; Han et al., 2014; Oke et al., 2017; Qian et al., 2022). Because urban population has increased rapidly and is expected to keep increasing (United Nations, 2019), there is a growing need for more reliable precipitation prediction and water management in cities and surrounding areas. To satisfy this need, first of all, much understanding of urban effects on precipitation is required.

Three causative factors for urban-induced or urban-modified precipitation have been suggested. Han et al. (2014) provided a review of the three factors and their roles. The first factor is the urban heat island which induces updrafts, initiates convection, and produces precipitation over or downwind of cities (Hjelmfelt, 1982; Bornstein and Lin, 2000; Baik et al., 2001; Han and Baik, 2008; Seino et al., 2018; Doan et al., 2021). The second factor is the large roughness of urban surfaces which decelerates or bifurcates air flow over cities. The changes in air flow due to the large roughness may decrease precipitation in cities and increase precipitation in surrounding areas (Bornstein and LeRoy, 1990; Dou et al., 2020; Dou et al., 2015). The last factor is the abundance of anthropogenic aerosols over cities which changes cloud microphysical and dynamical processes, leading to changes in urban precipitation (Rosenfeld,

\* Corresponding author.

E-mail address: [jjbaik@snu.ac.kr](mailto:jjbaik@snu.ac.kr) (J.-J. Baik).

2000; Ntelekos et al., 2009; Han et al., 2012; Ochoa et al., 2015; Schmid and Niyogi, 2017). The relative importance of these three factors for urban-induced or urban-modified precipitation varies depending on the geographical locations of cities and synoptic or mesoscale weather conditions.

Observational studies have reported several characteristics of precipitation in and around cities. A review of observational studies in many cities showed that precipitation amounts in or downwind of cities are about 20% larger on average than those in control regions where urban influences are negligible (Liu and Niyogi, 2019). The review also showed that the precipitation increase occurs on average 45–55 km downwind of the city center. Many studies reported that the precipitation increase in or downwind of cities is especially prominent for short and heavy precipitation events (e.g., Wu et al., 2019) and summer precipitation events (e.g., Changnon, 1979; Changnon et al., 1991; Daniels et al., 2016). In addition to those aforementioned, other characteristics of precipitation in and around cities such as a decrease in light precipitation in a city (Yang et al., 2021) and winter precipitation increases in cities (Manola et al., 2020) were reported.

The observed precipitation increases downwind of cities have been studied as a major characteristic of precipitation around cities. Huff and Changnon (1972) reported that the precipitation amount in the climatologically downwind region of St. Louis, USA are 9% larger than that in the climatologically upwind region. Changnon (1979) and Changnon et al. (1991) showed that the increase in precipitation amount downwind of St. Louis is largest in summer, followed by fall and spring. Diem and Mote (2005) compared the spatial pattern of summer precipitation in and around Atlanta, USA during the less-urbanized period with that during the more-urbanized period. They found that the number of heavy precipitation days in the northeastern Atlanta metropolitan area which is the climatologically downwind region of downtown Atlanta for heavy precipitation events is significantly increased between the two periods. Hand and Shepherd (2009) examined the spatial distribution of accumulated precipitation amount in and around Oklahoma City, USA over the days with weak synoptic forcing during June–September and showed that the maximum precipitation amount is observed in the climatologically downwind region of the city. Takahashi et al. (2011) reported the frequency maxima of intense precipitation downwind of Shinjuku, Ikebukuro, and Shibuya wards in Tokyo, Japan. Yang et al. (2014) showed that a high frequency of heavy precipitation events appears in the climatological downwind region of the urban core of Beijing, China. Daniels et al. (2016) categorized daily precipitation amounts along the west coast of the Netherlands according to the estimated wind directions at 12 UTC. They showed that daily precipitation amounts are larger downwind of cities for sufficiently strong winds and are larger in the regions surrounded by cities for weak winds.

Although the downwind precipitation increases have been extensively investigated, more rigorous examinations with high spatial and temporal resolution data are further required to better detect urban effects on precipitation. Lowry (1998) pointed out that to objectively assess whether precipitation maxima really occur downwind of cities, a dense rain gauge network is necessary. However, using more rain gauges in a study usually reduces the length of time period shared by the rain gauges, which can cause a problem in identifying the climatological characteristics of precipitation in and around cities (Braham, 1979). There are few studies in which both a long data period and a high density of rain gauges are used (e.g., Takahashi et al., 2011; Daniels et al., 2016). Moreover, except for, for example, the Metropolitan Meteorological Experiment (METROMEX) project (Vogel and Huff, 1978; Changnon, 1979; Changnon et al., 1991), which used hourly wind data, most studies employed the low-level wind direction at 12 UTC for each day and/or that averaged over a long period of time to determine the downwind region of a city (Shepherd et al., 2002; Diem and Mote, 2005; Hand and Shepherd, 2009; Keuser, 2014; Daniels et al., 2016). It is expected that wind data with a higher temporal resolution (e.g., hourly) could provide more representative wind directions for individual precipitation events.

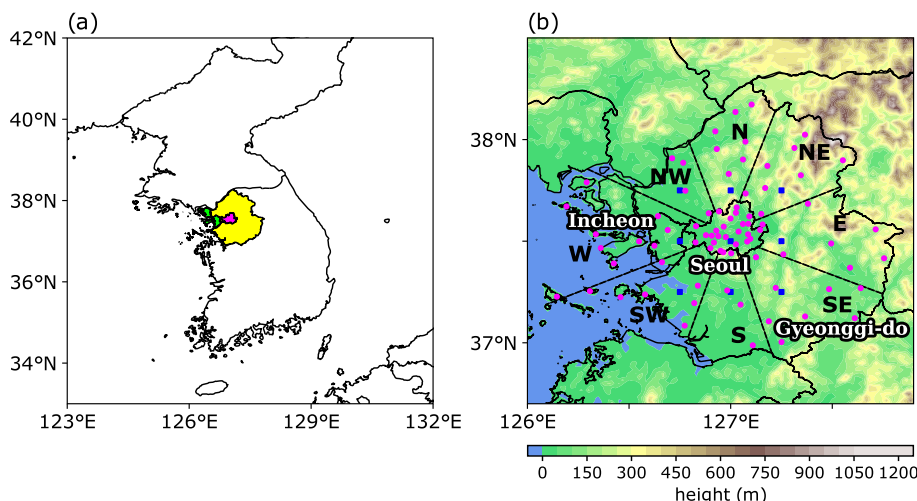


**Fig. 1.** (a) Location of the Seoul Metropolitan Area (SMA) which comprises Seoul, Incheon, and Gyeonggi-do (colored in magenta, green, and yellow, respectively). (b) Topographic map of the SMA with the locations of 80 rain gauge stations (magenta circles) and 9 grid points of ERA5 850-hPa wind data in and around Seoul (blue rectangles). (For interpretation of the references to colour in this figure legend, the reader is referred to the web version of this article.)

The Seoul Metropolitan Area (SMA), South Korea, which includes megacity Seoul, has a dense rain gauge network with a sufficient time length of data, which makes it possible to identify the spatiotemporal patterns of precipitation in detail. Thus, the SMA can be a good place to study urban effects on precipitation. Kim et al. (2011) examined the spatial distribution of precipitation in the SMA using a dense rain gauge network. A large amount of heavy precipitation was seen in the northeastern SMA which is the climatologically downwind region of Seoul in summer. In their study, precipitation events are not categorized according to the low-level wind directions. By categorizing precipitation events according to the low-level wind directions, the region of a relatively large amount of precipitation is expected to vary with the low-level wind direction, which will show urban effects on precipitation in the SMA in more detail.

This study aims to detect urban effects on precipitation in the SMA using long-term high-density precipitation data and considering low-level wind directions with high temporal resolution wind data. In section 2, data and analysis methods are described. In section 3, analysis results are presented and discussed. A summary and conclusions are given in section 4.

## 2. Data and methods

### 2.1. Study area

The SMA is located in the central west of the Korean Peninsula (Fig. 1a). It comprises three administrative divisions: Seoul, Incheon, and Gyeonggi-do (Fig. 1b). The SMA has complex geographical features. A mountainous region whose peak height is 1212 m is in the northeastern region of the SMA and extended further northeastward (Fig. 1b). The Yellow Sea is located west of the SMA. The climate of the SMA is characterized by hot and humid summer. The mean annual precipitation amount in the SMA during 2005–2020 is 1262 mm. Summer precipitation accounts for 62% (781 mm) of the annual precipitation amount. The Changma front (a quasi-stationary front causing a large amount of precipitation over the Korean Peninsula during the East Asian summer monsoon), typhoons, and isolated showers characterize the summer precipitation.

Seoul is the most urbanized region in the SMA and has a population of about 10 million. Its population density is about 11 times that of the rest of the SMA. Although there are densely populated and built-up regions in other cities as well, the sizes of those regions are smaller than those in Seoul. Therefore, in this study, we aim to detect the effect of the megacity Seoul on precipitation in the SMA. The urban heat island intensity of Seoul in summer is maximum (about 2.5 °C) in the midnight (00–03 LST) and minimum (about 0.4 °C) in the late afternoon (15–18 LST) (Lee and Baik, 2010). In terms of the roughness of urban surfaces, there are about 980 buildings per 1 km<sup>2</sup> in Seoul and 20% of them are taller than five floors (<https://kosis.kr>). The average roughness length of Seoul is estimated to be 1.5 m (Yi et al., 2015). The annual mean concentrations of particulate matter with diameters smaller than 10 µm (PM<sub>10</sub>) and 2.5 µm (PM<sub>2.5</sub>) in Seoul during 2011–2018 are about 45 and 23 µg m<sup>-3</sup>, respectively (Yeo and Kim, 2019).

### 2.2. Data

In this study, hourly precipitation data during 2005–2020 from a rain gauge network in the SMA are used. From the rain gauge network, data from 80 rain gauges with missing data less than 3.5% of the total data are used for analysis (Fig. 1b). Those missing data are excluded from analysis. Hourly 850-hPa horizontal wind data from the European Centre for Medium-Range Weather Forecasts Reanalysis version 5 (ERA5, Hersbach et al., 2020) at nine grid points in and around Seoul (Fig. 1b) are used to categorize precipitation events based on low-level wind types and to examine the evolutions of precipitation systems for different low-level wind types.

### 2.3. Methods

A precipitation event for a given station is defined as an event during consecutive hours of which the hourly precipitation amount exceeds 0.1 mm (Yang et al., 2017). The precipitation amount and duration of a precipitation event are defined as the accumulated precipitation amount and accumulated number of hours during the event, respectively. The intensity of a precipitation event is defined as the precipitation amount of the event divided by the duration of the event.

Precipitation events are categorized according to the types of low-level wind averaged over 3 h prior to each precipitation event: weak (< 3 m s<sup>-1</sup>), W, SW, S, SE, E, NE, N, and NW types. The 850-hPa wind averaged over the nine grid points in and around Seoul is used as the low-level wind (Fig. 1b). The SMA is also divided into nine regions: Seoul, W, SW, S, SE, E, NE, N, and NW regions. For each wind type, upwind and downwind regions of Seoul are determined among the nine regions and the precipitation amounts in these two regions are compared. For example, for the W wind type, the upwind region is the W region and the downwind region is the E region. For the weak wind type, precipitation amounts are compared between Seoul and the rest of the SMA because the former is expected to experience urban effects more than the latter. For convenience, the two regions are assigned the downwind and upwind regions, respectively. To test the significance of differences in accumulated precipitation amount and frequency between the upwind and downwind regions, the paired Student's *t*-test is used for half-monthly accumulated values. To test the significance of differences in mean duration and mean intensity of precipitation events, the unpaired Student's *t*-test is used.

For each wind type, precipitation events are further classified by their durations and intensities to identify which types of events mainly contribute to the precipitation difference between the upwind and downwind regions. The durations of events are classified into short (1–6 h), middle (7–12 h), and long ( $\geq 13$  h) classes. The intensities (*I*) of events are classified into light ( $I < 0.6 \text{ mm h}^{-1}$ ), moderate ( $0.6 \text{ mm h}^{-1} \leq I < 2.5 \text{ mm h}^{-1}$ ), heavy ( $2.5 \text{ mm h}^{-1} \leq I < 15 \text{ mm h}^{-1}$ ), and extreme ( $\geq 15 \text{ mm h}^{-1}$ ) classes.

To compare the spatial patterns of precipitation amount for different wind types, the rural-to-urban ratio is calculated following

Huff and Changnon (1972) and Lowry (1998). The rural-to-urban ratio is a normalized precipitation amount which is computed by dividing the accumulated precipitation amount at each station by that averaged over Seoul for each wind type.

To identify what kinds of precipitation systems are related to the precipitation increase associated with urban effects, composite fields of hourly precipitation amount and low-level wind are examined some hours before and after the beginning times of the precipitation events in the SMA. The composite field at each time is obtained by weighted averaging, where the fields at that time are averaged over all precipitation events in the SMA and the accumulated precipitation amount of each precipitation event is used as the weight.

### 3. Results and discussion

#### 3.1. Seasonal characteristics

**Fig. 2** shows the spatial distributions of annual and seasonal mean precipitation amounts in the SMA during 2005–2020. The annual mean precipitation amount generally increases from west to east in the SMA (**Fig. 2a**). The region of the largest precipitation amount varies with the season. The precipitation amount is largest in the E region in spring (**Fig. 2b**), the NE region in summer (**Fig. 2c**), and the SE region in fall (**Fig. 2d**) and winter (**Fig. 2e**). The mean wind at 850 hPa in and around Seoul is westerly in spring, southwesterly in summer, westerly in fall, and northwesterly in winter. Thus, the region of the largest precipitation amount is the downwind region or the region just beside the downwind region in each season. The agreement between the region of the largest precipitation amount and the climatologically downwind region was also found for many cities in USA (Shepherd et al., 2002; Keuser, 2014). Seoul also exhibits a large precipitation amount in summer and fall, although the precipitation amount is not as large as precipitation amounts in the NE and SE regions. The large precipitation amounts found in Seoul, its downwind region, and/or the region just beside the downwind region can be associated with precipitation enhancement due to urban effects. It should be also considered that for summer, the large precipitation amount in the downwind (NE) region may also be affected by the mountains there.

The monthly variations of precipitation amounts in the upwind and downwind regions and the relative difference between them are presented in **Fig. 3**. The precipitation amount is largest in July in both the upwind and downwind regions, and the difference in precipitation amount between the upwind and downwind regions is largest in August (**Fig. 3a**). May, June, July, and August show statistically significant increases in precipitation amount in the downwind region (at a significance level of 0.05) (**Fig. 3b**). The relative difference is largest in August (64%), followed by July (31%) and May (22%). Among all seasons, summer shows the largest increase in precipitation amount (39%), which is statistically significant. The increase in precipitation amount in spring (9%) is also statistically significant, but those in fall (4%) and winter (4%) are not statistically significant.

The magnitude of downwind increase in precipitation amount can be different depending on the temporal resolution of precipitation and wind data. If the downwind region is determined using the low-level wind at 12 UTC for each day or the low-level wind averaged over each month instead of hourly data, the relative difference in precipitation amount is calculated as 48% or 27%, respectively, which is considerably different from that obtained using the hourly data in this study (39%). Thus, the comparison of the

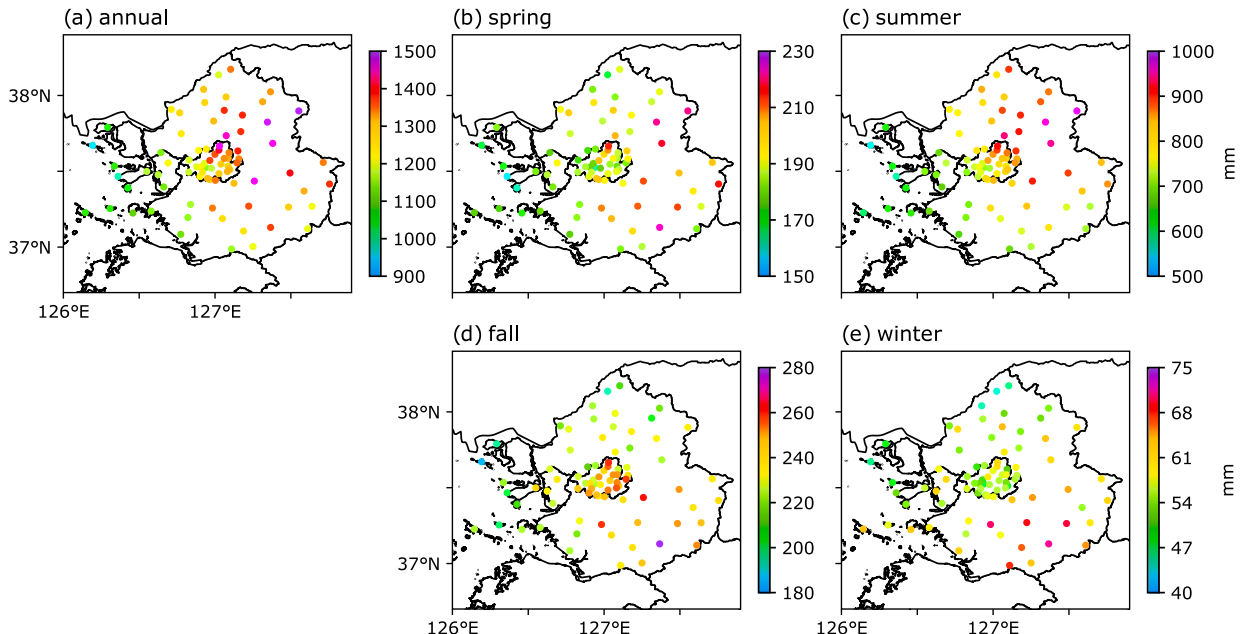


**Fig. 2.** Spatial distributions of (a) annual mean precipitation amount and seasonal mean precipitation amounts for (b) spring, (c) summer, (d) fall, and (e) winter in the SMA during 2005–2020.

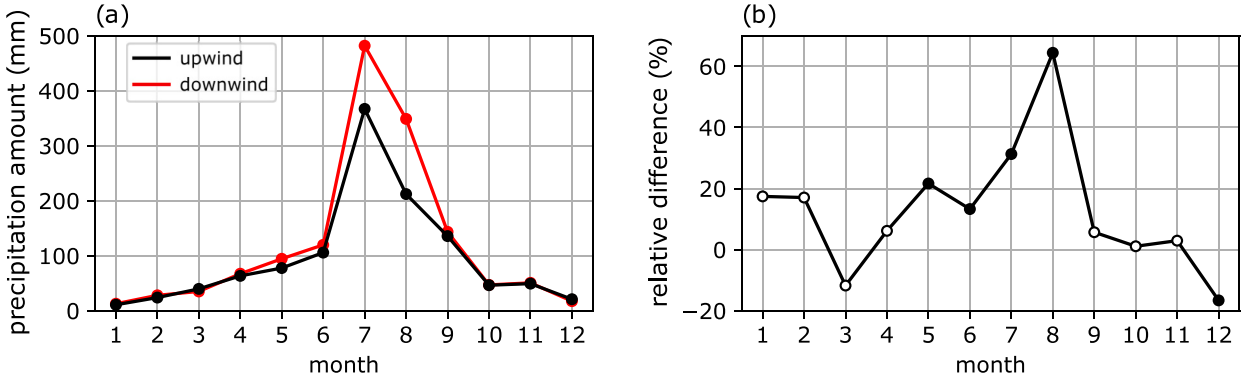


**Fig. 3.** (a) Monthly mean precipitation amounts in the upwind and downwind regions and (b) the relative difference between them (downwind minus upwind) in each month. In (b), filled (open) circles denote statistically significant (insignificant) increase or decrease from the upwind to downwind regions.

magnitudes of increase in precipitation amount associated with urban effects between studies with different temporal resolutions of data should be done with caution.

The spatial distribution of the rural-to-urban ratio in summer during 2005–2020 is presented for each wind type (Fig. 4). Here, only the wind types for which the accumulated precipitation amounts averaged over the SMA are greater than 100 mm are considered in order to exclude the wind types that are dominated by a small number of precipitation events. As a result, the NW, N, and NE wind types are excluded from analysis. The accumulated precipitation amount for the remaining six wind types accounts for 99% of the total, and that for the SW wind type accounts for the largest portion (47%), followed by the S wind type (25%). The rural-to-urban ratio is highest in the downwind region for four (weak, W, SW, and S) out of the six wind types. For the SW wind type, the high rural-to-

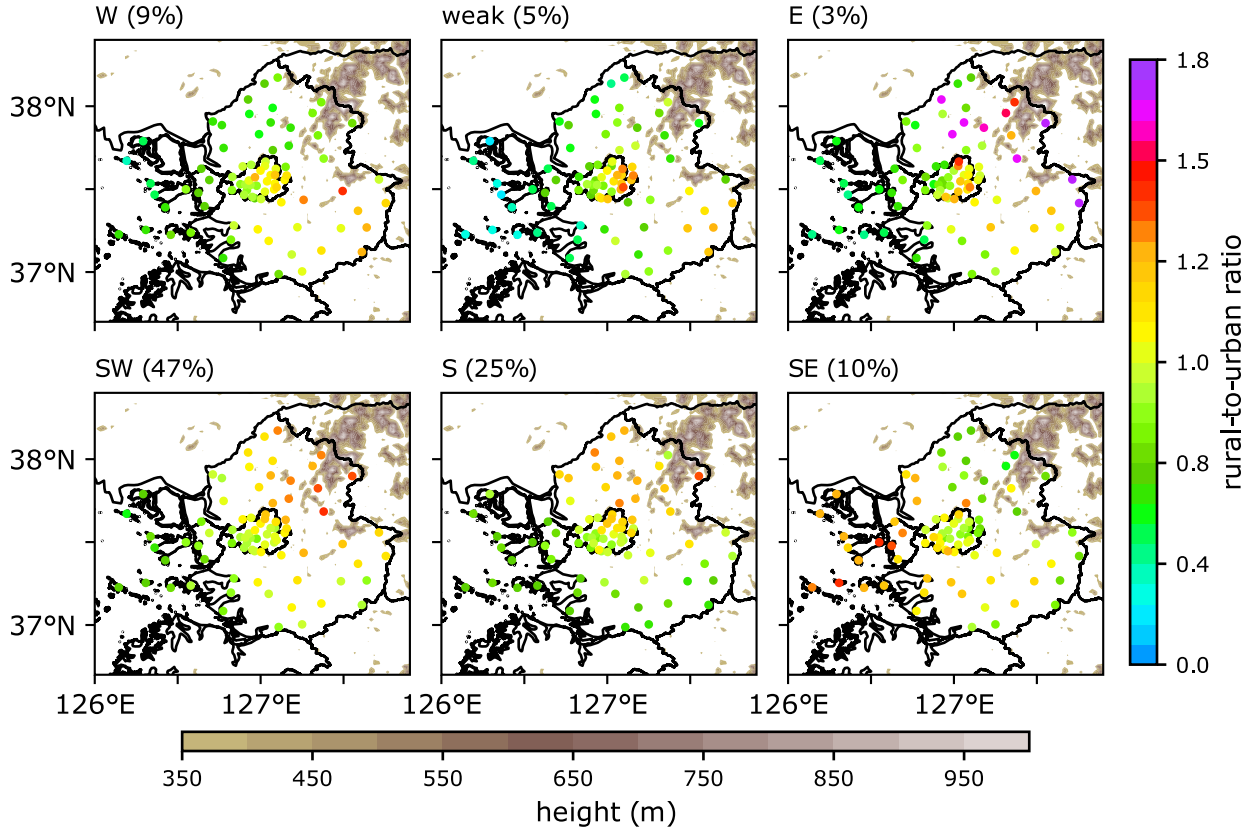


**Fig. 4.** Spatial distribution of the rural-to-urban ratio in the SMA in summer during 2005–2020 for each wind type with a sufficient accumulated precipitation amount (the accumulated precipitation amount averaged over the SMA > 100 mm). The percentage value in each subfigure represents the accumulated precipitation amount averaged over all stations in the SMA for each wind type divided by that for all wind types.

urban ratio in the downwind region may also be associated with topographic effects on precipitation in the NE region. For the SE wind type, the rural-to-urban ratio is highest in the W region, located just beside the downwind region. Unlike other wind types, the rural-to-urban ratio for the E wind type is highest in the E region, not in the downwind region or the region just beside the downwind region. The downwind increases in rural-to-urban ratio for the weak, W, SW, S, and SE wind types are statistically significant, while that for the SE wind type is not. For the E wind type, the rural-to-urban ratio is smaller in the downwind region than in the upwind region.

For the five wind types that show the downwind precipitation increase (the weak, W, SW, S, and SE wind types), the overall downwind increase is 45%. This value changes only slightly when the SW wind type, which the topographic effects may be involved in, is excluded (40%). For reliable estimation of the topographic effects reflected in the downwind precipitation increase, further investigation using a numerical model in which land-use types and topography can be changed independently is needed.

The spatial distribution of the rural-to-urban ratio for each wind type is also examined for spring, fall, and winter (not shown). Although these three seasons show downwind increases in rural-to-urban ratio, the highest rural-to-urban ratio mostly does not appear in the downwind region in these seasons. Thus, among all seasons, it appears that summer shows the most prominent signals of precipitation increase associated with urban effects. This qualitatively agrees with the result of Kug and Ahn (2013) that the correlation between the precipitation increase and the population growth in cities in South Korea is distinctively higher in summer than in other seasons. The prominent signals in summer in the SMA are associated with the climatological features of summer. In South Korea, it is hot and humid in summer and convective precipitation comprises a relatively large portion of summer precipitation compared to the precipitation in other seasons (Suh et al., 2016). Vogel and Huff (1978) and Changnon et al. (1991) suggested that the precipitation increase in the downwind region of a city is more prominent for convective precipitation than for the other types of precipitation. In South Korea, among the three months of summer, August is especially characterized by high near-surface temperature, weak synoptic forcing, and relatively frequent occurrence of isolated showers unlike June and July when the Changma front plays an important role in producing precipitation on a much larger horizontal scale. Ashley et al. (2012) and Haberlie et al. (2015) suggested that thunderstorm initiation increases in urban areas under weak synoptic forcing, from which August is expected to show distinct urban effects on precipitation. The results in this subsection encourage to look into the precipitation characteristics in August in detail, which are shown in the next subsection.

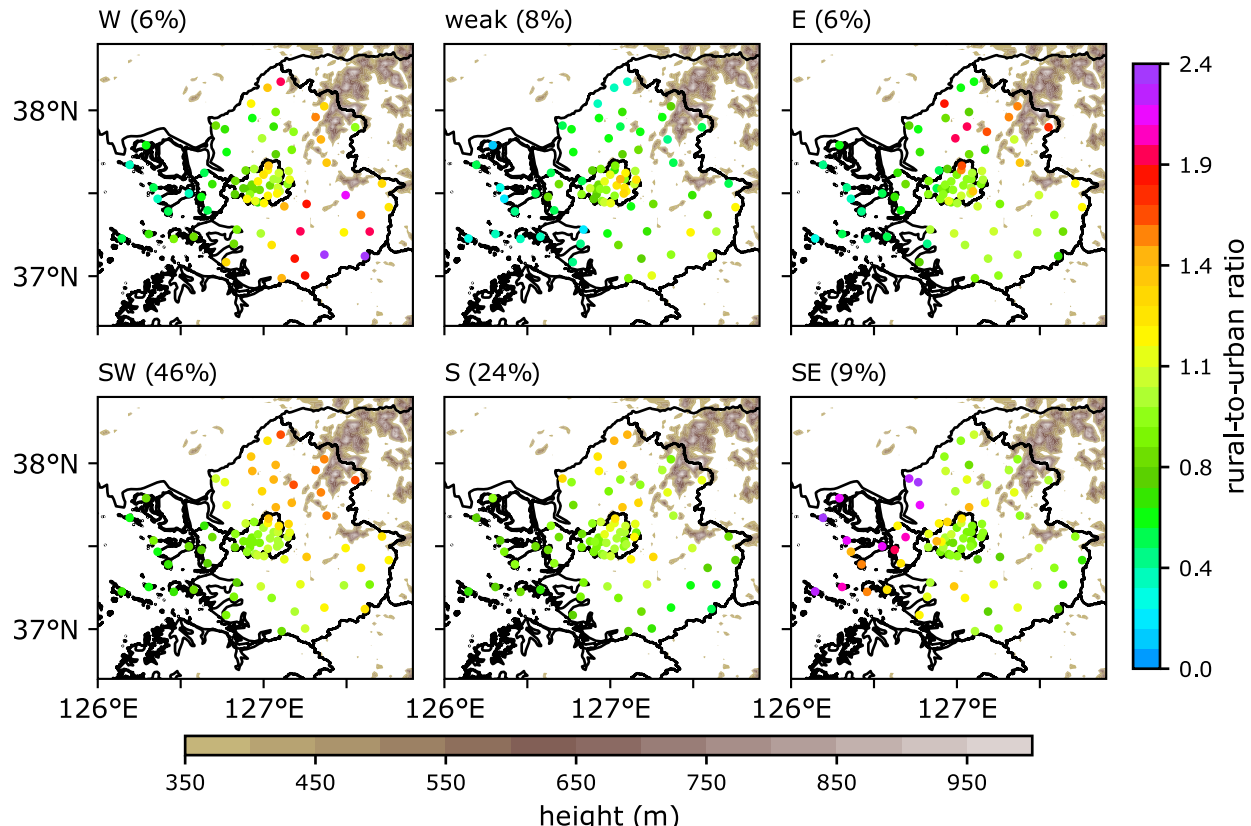


**Fig. 5.** As in Fig. 4, but for August.

### 3.2. Characteristics of precipitation in August

#### 3.2.1. Analysis of downwind precipitation increase

[Fig. 5](#) shows the spatial distributions of the rural-to-urban ratio of accumulated precipitation amount in the SMA in August during 2005–2020 for the weak, W, SW, S, SE, and E wind types. The NW, N, and NE wind types are excluded from analysis for the same reason as in summer. The accumulated precipitation amount for the six wind types accounts for 99% of the total. The accumulated precipitation amount for the SW wind type accounts for the largest portion (46%), followed by the S wind type (24%). For each wind type, the spatial pattern of the rural-to-urban ratio in August is generally similar to that in summer. The rural-to-urban ratio is highest in the downwind region for four (weak, SW, S, and SE) out of the six wind types. For the W wind type, the rural-to-urban ratio is highest in the SE region, located just beside the downwind region. The rural-to-urban ratio for the E wind type is highest in the NE region. The rural-to-urban ratio in the downwind region averaged over the wind types except for the E wind type in August (1.45) is much higher than that in summer (1.15), indicating that the precipitation increase associated with urban effects is much more pronounced in August. The rural-to-urban ratio in the downwind region averaged over the five wind types is similar to that calculated excluding the SW wind type (1.44).

The location of the maximum precipitation increase in the downwind region is also an important aspect in urban effects on precipitation. For the W, SW, S, and SE wind types that show a precipitation increase in the downwind region, the rural-to-urban ratio at each station in the downwind region is presented as a function of the distance from the center of Seoul ([Fig. 6](#)). For the W and SE wind types, the rural-to-urban ratio in the downwind region is highest at 40–50 km from the center of Seoul. For the W wind type, the highest rural-to-urban ratio is 2.2 at 46 km from the center of Seoul. For the SW and S wind types, the rural-to-urban ratio is highest more than 60 km away from the center of Seoul. [Liu and Niyogi \(2019\)](#) reported that the downwind precipitation increases in previous observational studies appear on average 45–55 km downwind of the city center. A more rigorous examination on this may be possible if the rain gauge network in the SMA becomes further denser in the future.

To examine the difference in diurnal variations of hourly precipitation amounts in the upwind and downwind regions, those for the weak, W, SW, S, and SE wind types are plotted in [Fig. 7](#). For the weak wind type, both the upwind and downwind regions show relatively large amounts of precipitation in the afternoon. The downwind precipitation increase is pronounced in the late afternoon (17–20 LST). This is consistent with the result of a numerical modeling study by [Doan et al. \(2021\)](#) which showed an increase in late afternoon precipitation. They suggested that the urban heat island is a possible cause of the precipitation increase in the late afternoon. For the W wind type, the downwind precipitation increase occurs at all times and it is considerable from the nighttime to afternoon and strongest in the early afternoon (12–15 LST). For the SW wind type, the downwind precipitation increase occurs at all times. The S and SE wind types show relatively large amounts of precipitation in the nighttime and morning in both the upwind and downwind regions. [Jin et al. \(2022\)](#) suggested that in summertime, the precipitation peaks in the late night-to-morning in South Korea are associated with large-scale systems. For the S wind type, the downwind precipitation increase mainly occurs in the nighttime and early morning (23–09 LST). For the SE wind type, the downwind precipitation increase is pronounced in the nighttime and early morning (22–08 LST) and also considerable in the late morning and afternoon (10–18 LST).

The relative differences in the accumulated precipitation amount, accumulated frequency, mean duration, and mean intensity of

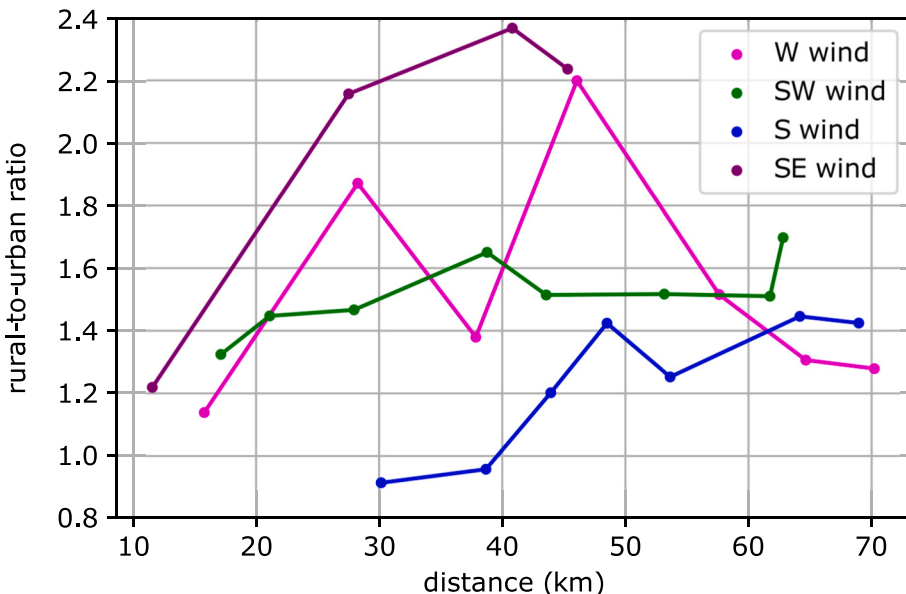


**Fig. 6.** Rural-to-urban ratio of accumulated precipitation amount at each station in the downwind region in August during 2005–2020 as a function of the distance of the station from the center of Seoul (37.56°N, 126.98°E) for the W, SW, S, and SE wind types which show a precipitation increase from the upwind to downwind regions.

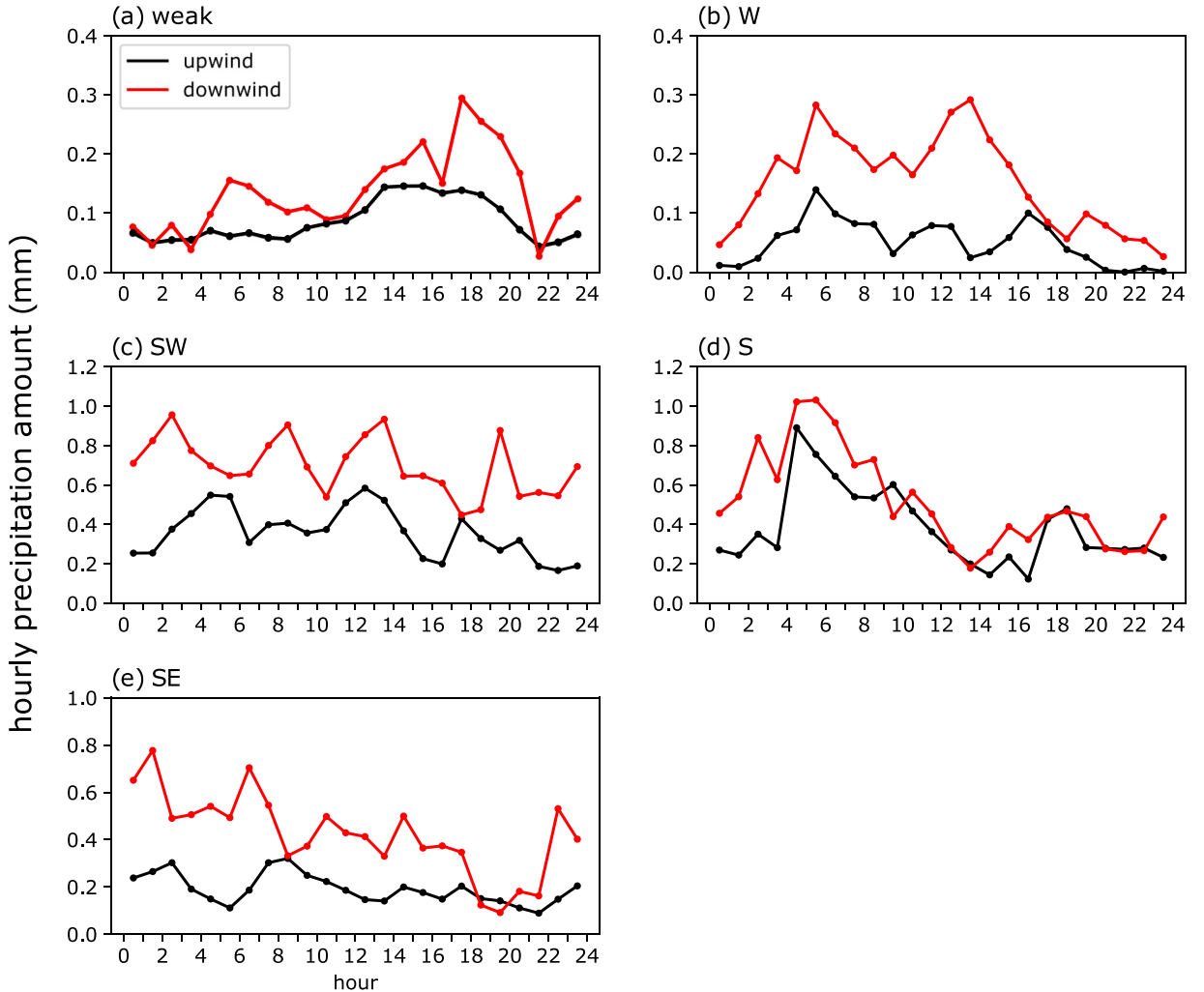


**Fig. 7.** Diurnal variations of hourly precipitation amounts in the upwind and downwind regions in August during 2005–2020 for the (a) weak, (b) W, (c) SW, (d) S, and (e) SE wind types which show a precipitation increase from the upwind to downwind regions.

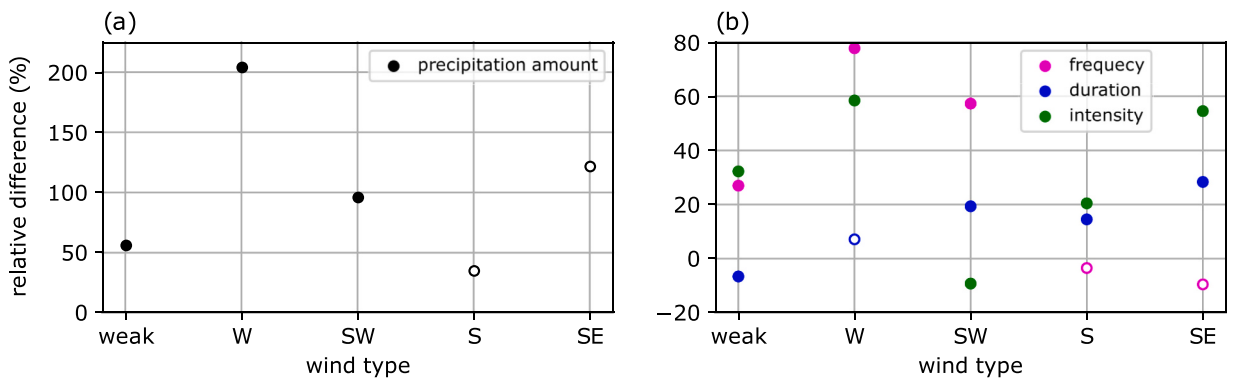


**Fig. 8.** Relative differences in (a) accumulated precipitation amount, (b) accumulated frequency, mean duration, and mean intensity of precipitation events between the upwind and downwind regions (downwind minus upwind) in August during 2005–2020 for the weak, W, SW, S, and SE wind types which show a precipitation increase from the upwind to downwind regions. Filled (open) circles denote statistically significant (insignificant) increase or decrease.

precipitation events between the upwind and downwind regions for the five wind types are shown in Fig. 8. The mean duration and intensity of a region are calculated by averaging the durations and intensities of individual precipitation events that occurred in the region, respectively. The precipitation increase is largest for the W wind type (204%) and smallest for the S wind type (35%) (Fig. 8a). The downwind precipitation increases for the weak, W, and SW wind types are statistically significant. Interestingly, the relative importance of the frequency, duration, and intensity to the increase in accumulated precipitation amount varies with the wind type (Fig. 8b). For the weak and W wind types, statistically significant increases in the accumulated frequency and mean intensity of precipitation events are responsible for the precipitation increases. For the SW wind type, statistically significant increases in the accumulated frequency and mean duration of precipitation events are responsible for the precipitation increase. For the S and SE wind types, statistically significant increases in the mean duration and intensity of precipitation events contribute to the precipitation increases. Considering the major contributors to the precipitation increase for each wind type, hereafter, the five wind types are grouped into three wind groups: Group 1 (the weak and W wind types), Group 2 (the SW wind type), and Group 3 (the S and SE wind types).

From that the major contributors to the precipitation increase are different for each wind group, it is implied that the types and evolutions of precipitation systems may also be different for each wind group. For Group 1, precipitation events occur more frequently and intensely in the downwind region than in the upwind region. This implies that precipitation systems are initiated or intensified in the downwind region. For Group 2, precipitation events occur more frequently and persist longer in the downwind region than in the upwind region, implying that precipitation systems are initiated or stay longer in the downwind region. For Group 3, precipitation events occur more intensely and persist longer in the downwind region than in the upwind region. Because the frequency of precipitation events shows no significant difference between the upwind and downwind regions, long-lasting precipitation systems that pass both the downwind and upwind regions but intensify and stay longer in the downwind region may be a possible candidate responsible for the precipitation increase from the upwind to downwind regions for Group 3. The characteristics and evolutions of precipitation systems for each wind group are investigated in the next subsection.

To identify what kinds of precipitation events are responsible for the precipitation increase from the upwind to downwind regions for the five wind types, precipitation events are classified into different duration classes and intensity classes. The contribution of each class to the precipitation increase is shown in Fig. 9. For the duration classes, the class that contributes most to the downwind precipitation increase varies with the wind group (Fig. 9a). For Group 1, short-duration events mainly contribute to the downwind precipitation increase while the contribution of long-duration events is negligible. A short-duration event can be caused by a precipitation system that lasts short, moves fast, or has a small size, etc. For the weak wind type in Group 1, the contributions of short-, middle-, and long-duration events are 70%, 27%, and 3%, respectively. For Group 2, middle-to-long-duration events mainly contribute to the downwind precipitation increase. This indicates that the precipitation systems responsible for the precipitation increase in Group 2 may last longer, move slower, or have larger sizes than those for Group 1. For Group 3, long-duration events contribute most to the downwind precipitation increase, which implies that the precipitation systems responsible for the precipitation increase in Group 3 may last further longer, move further slower, or have further larger sizes than those for Group 1 and Group 2. For the intensity classes, the class that most contributes to the downwind precipitation increase for the weak, W, SW, and SE wind types is heavy precipitation and that for the S wind type is extreme precipitation (Fig. 9b). Results that are similar to those for Group 1 were reported in Beijing (Yang et al., 2017) and the Pearl River Delta region (Wu et al., 2019), China, where the amount and frequency of short-duration and heavy precipitation increase in urban area. They suggested that it is closely associated with the urban heat island.

### 3.2.2. Characteristics and evolutions of precipitation systems

To compare the average sizes of precipitation systems for the five wind types, the time series of average number of SMA stations where precipitation occurs are plotted in Fig. 10 for the period from 2 h before to 6 h after the beginning time of precipitation events in the SMA. Before the beginning time, the average number of stations increases with time, and it is maximized at or 1 h after the beginning time. The maximum average number is largest in the S wind type (37), followed by the SE (35), SW (33), weak (24), and W (24) wind types. It is noted that the maximum average number for each wind type in Group 1 is much smaller than those for the wind

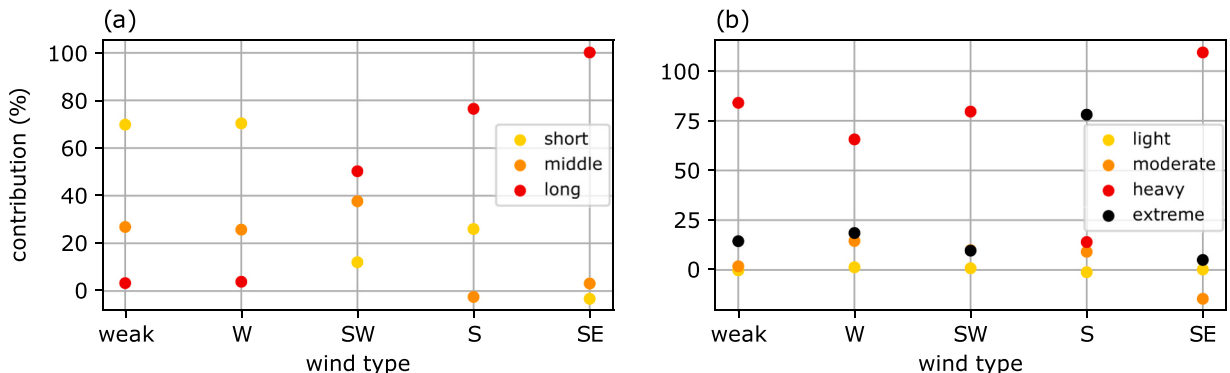


**Fig. 9.** Contributions of precipitation events in different (a) duration classes and (b) intensity classes to the downwind precipitation increase in August during 2005–2020 for the weak, W, SW, S, and SE wind types which show a precipitation increase from the upwind to downwind regions.

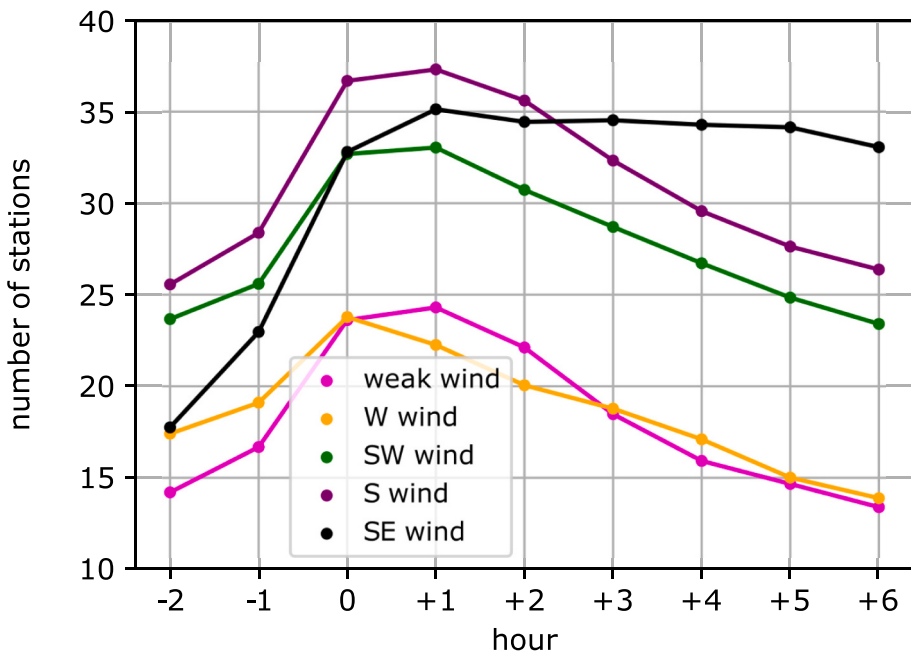


**Fig. 10.** Time series of average number of SMA stations where precipitation occurs from 2 h before to 6 h after the beginning time of precipitation events in the SMA for the weak, W, SW, S, and SE wind types.

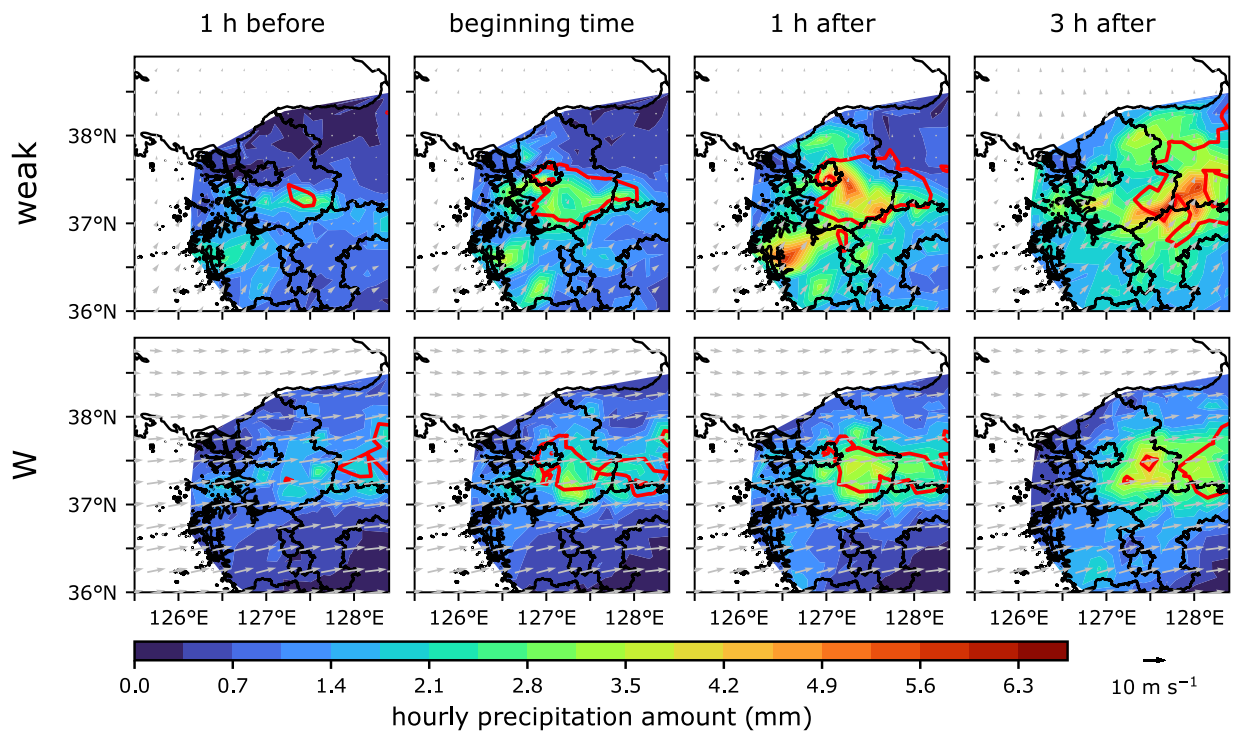


**Fig. 11.** Composite fields of hourly precipitation amount (shaded) and 850-hPa wind vector 1 h before the beginning time, at the beginning time, and some hours after the beginning time of precipitation events in the SMA for the wind types in Group 1. The areas inside the red contours indicate areas where more than one third of the precipitation events in the SMA occur. (For interpretation of the references to colour in this figure legend, the reader is referred to the web version of this article.)

types in Group 2 and Group 3. 2 h after the beginning time, the average number decreases except for the SE wind type in Group 3. After the beginning time, the average number of stations where precipitation occurs for Group 1 accounts for a much smaller portion of the total number of SMA stations than those for Group 2 and Group 3. For example, 5 h after the beginning time, the portion of stations where precipitation occurs is 18% and 19% for the weak and W wind types in Group 1, respectively, 31% for the SW wind type in Group 2, and 35% and 43% for the S and SE wind types in Group 3, respectively. This indicates that precipitation systems associated with the downwind precipitation increase for Group 1 have much smaller sizes than those for Group 2 and Group 3. Because small-sized precipitation systems can result in a relatively short duration of precipitation event, the above result can give an explanation for the large contribution of short-duration precipitation events to the downwind precipitation increases for the wind types in Group 1 (Fig. 9a).

Composite fields of hourly precipitation amount and 850-hPa wind in and around the SMA for the five wind types are presented to examine the characteristics and evolutions of precipitation systems for each wind type (Figs. 11–13). For this, 1 h before the beginning time, the beginning time itself, and 1 h (1 h and 2 h) and 3 h (4 h and 6 h) after the beginning time are selected for Group 1 (Group 2 and Group 3). The areas inside the red contours are areas where precipitation occurs for more than one third of the precipitation events in the SMA, which give a rough estimation on the evolution of precipitation area representative of each wind type. For these figures, hourly precipitation data from 140 rain gauges outside of the SMA are additionally used.

For Group 1 (the weak and W wind types), only small amounts of precipitation are observed in the downwind region before the beginning time of precipitation events (Fig. 11). Large hourly precipitation amounts appear 1 h after the beginning time in the corresponding downwind regions for the two wind types. The size of areas inside the red contours becomes larger compared to the beginning time. At 3 h after the beginning time, the precipitation amount in the downwind region is largely reduced and the largest precipitation amount is observed outside of the SMA for the weak wind type. For the W wind type, at that time, the areas inside the red contour is moved eastward. These results suggest that the precipitation systems for Group 1 are mainly initiated in the SMA, are intensified within a short time, move rapidly to the east, and weaken. For the W wind type, the precipitation systems move approximately in the 850-hPa wind direction. The results from Figs. 8b, 9, 10, and 11 suggest that for Group 1, small-sized precipitation systems are initiated more frequently and develop more strongly in the downwind region than in the upwind region, producing short-duration and heavy precipitation more in the downwind region. Similar results were found by Fujibe et al. (2009), who reported a long-term increasing trend and a positive spatial anomaly of afternoon precipitation amount in the highly urbanized area in Tokyo, Japan for short-duration precipitation events without preceding precipitation in the warm season. For the same region, Seino et al. (2018) obtained similar results from the numerical simulations for August in 8 years. They found that the enhancement of convection due to the urban heat island circulation plays an important role in the precipitation increase.

For Group 2 (the SW wind type), large amounts of precipitation pre-exist near the downwind region before the beginning time of precipitation events (Fig. 12). At the beginning time, the region of large precipitation amounts and the area inside the red contour move southward from north of the SMA. At 1 h after the beginning time, large precipitation amounts appear in the downwind region and remains there for a long time thereafter while slowly decreasing. The size of area inside the red contour does not change much during the period. It is implied from the area inside the red contour that the precipitation systems for Group 2 cover a larger portion of the SMA than those for Group 1 (Fig. 11), which is consistent with the result that the portion of stations where precipitation occurs for Group 2 is larger than that for Group 1 (Fig. 10). This suggests that long-lasting and relatively large-sized precipitation systems are largely responsible for middle-to-long duration and heavy precipitation in the downwind region. Considering that the downwind region for Group 2 is the NE region including mountainous terrains, both urban effects and topographic effects may contribute to the large precipitation amount in the downwind region. The urban effects were separately identified from the topographic effects in a modeling study (Kusaka et al., 2019), but it is difficult to be done in an observational study.

For Group 3 (the S and SE wind types), there are some amounts of precipitation pre-existing at the west coast before the beginning time of precipitation events (Fig. 13). At the beginning time, the area in the red contour covers a large portion of the SMA. The precipitation systems enter the SMA from the west. At 2 h after the beginning time, the systems show large hourly precipitation amounts in the downwind region. These systems move slowly to the east, producing long-lasting precipitation in the downwind region (6 h after). These results suggest that long-lasting and large-sized precipitation systems are largely responsible for long-duration and heavy-to-extreme precipitation in the downwind region. Unlike for the wind types of different wind directions in Group 1 and Group 2, the wind direction changes during the analyzed hours for the wind types in Group 3. For example, the wind direction in the SMA changes slightly clockwise from southerly for the S wind type and from southeasterly for the SE wind type. This implies that there is a change in large-scale forcing that may contribute to the evolutions of precipitation systems for Group 3. The change in large-scale forcing during the analyzed hours makes it difficult to clearly identify the urban effects on the evolutions of precipitation systems for Group 3.

#### 4. Summary and conclusions

In this study, we attempted to detect urban effects on precipitation in the SMA, South Korea by analyzing hourly precipitation data from 80 rain gauges during 2005–2020. Precipitation events are categorized according to the low-level wind types, and precipitation in the upwind and downwind regions is compared. It is found that the precipitation increase in the downwind region is largest in summer (39%), especially in August (64%). Accordingly, the downwind precipitation increase in August is analyzed in detail. For the weak wind type, precipitation increases in Seoul, and for the W wind type, it increases 25–50 km downwind of the center of Seoul. The largest precipitation increase occurs in the afternoon. The accumulated frequency and mean intensity of precipitation events show an increase in the downwind region, which is responsible for the precipitation increase. For the weak and W wind types, the increase in

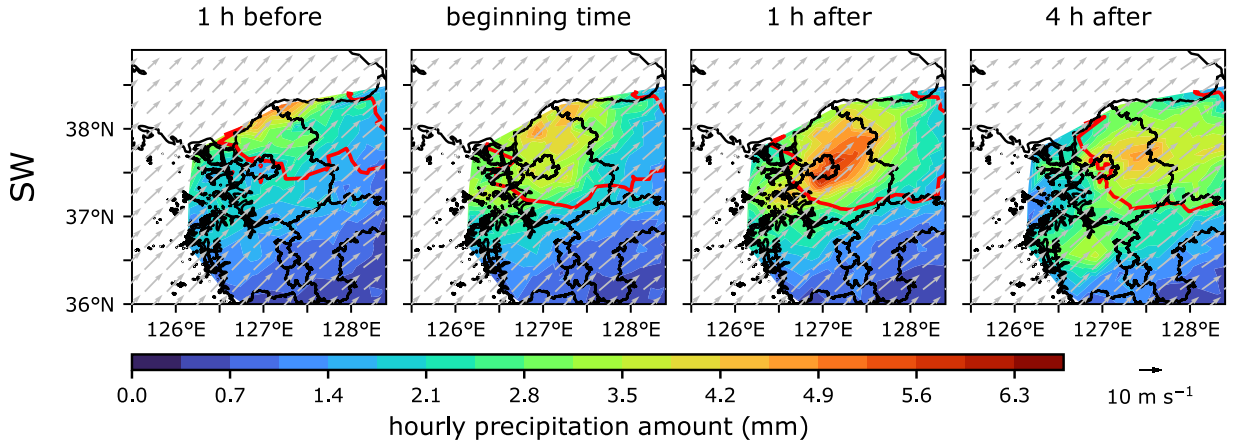


**Fig. 12.** As in Fig. 11, but for the wind type in Group 2.

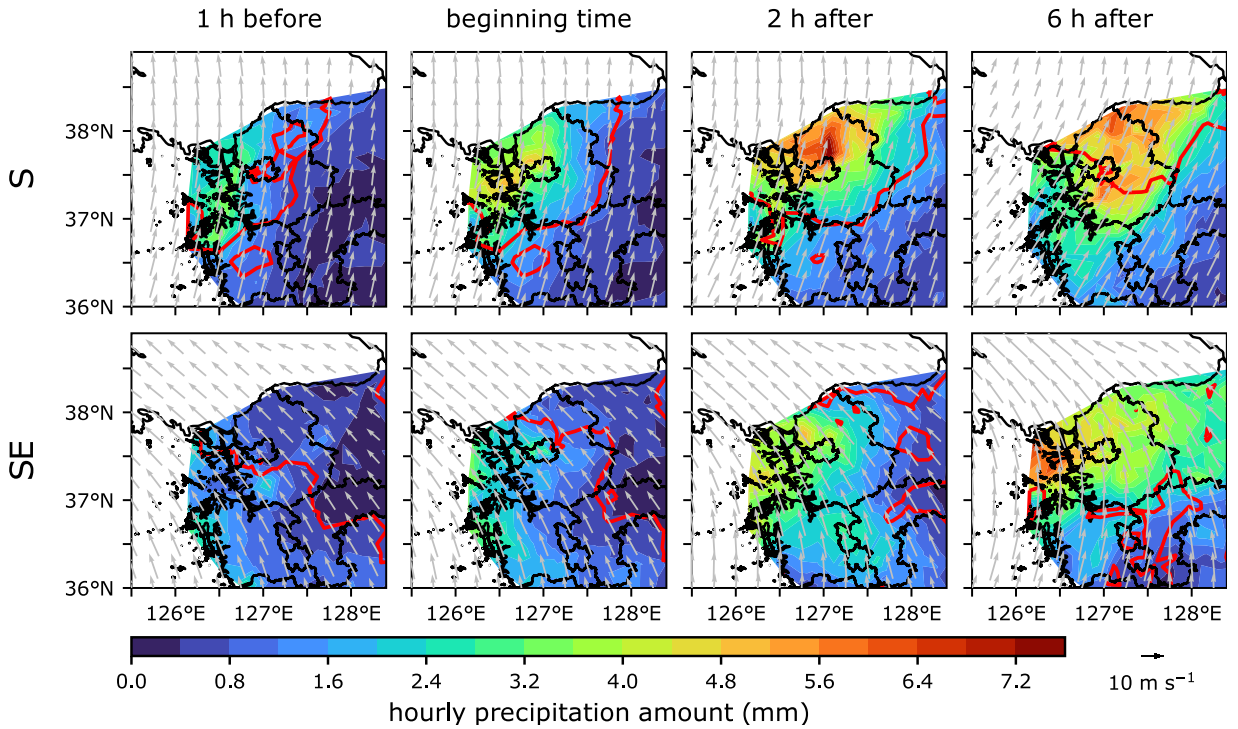


**Fig. 13.** As in Fig. 11, but for the wind types in Group 3.

short-duration and heavy precipitation is mainly responsible for the precipitation increase, which is associated with small-sized precipitation systems initiated within the SMA. For the SW, S, and SE wind types, the downwind precipitation increase also occurs. The increase in middle-to-long-duration precipitation is mainly responsible for the precipitation increase, which is associated with relatively large-sized precipitation systems entering from the outside of the SMA.

In this study, the downwind precipitation increase is examined in the SMA using precipitation data from a rain gauge network. However, it is difficult to detect the initiation and evolution of precipitation systems solely from the rain gauge data. Radar and satellite data with high spatial and temporal resolutions together with rain gauge data will greatly benefit this detection. Hence, the remote sensing data can be used in future investigation to better detect urban effects on precipitation.

This study reveals that the precipitation in the SMA shows a prominent downwind increase. However, besides the urban effects, inhomogeneous geographical features within and around the SMA such as the Yellow Sea and mountains may have affected the precipitation difference between the upwind and downwind regions. To distinguish the urban effects from other effects and to examine the interactions between them, a numerical modeling study is needed. The use of a sophisticated numerical model will also enable us to identify the relative importance of the three causative factors of urban effects (i.e., the urban heat island, large surface roughness, and

high aerosol concentration) on precipitation in the SMA.

## CRediT authorship contribution statement

**Seong-Ho Hong:** Formal analysis, Investigation, Writing – original draft, Visualization. **Han-Gyul Jin:** Formal analysis, Writing – original draft, Writing – review & editing. **Jong-Jin Baik:** Conceptualization, Formal analysis, Writing – review & editing, Supervision.

## Declaration of Competing Interest

The authors declare that they have no known competing financial interests or personal relationships that could have appeared to influence the work reported in this paper.

## Data availability

Data will be made available on request.

## Acknowledgements

We thank one anonymous reviewer for providing valuable comments on this work. The authors thank the Korea Meteorological Administration for providing the rain gauge data. This work was funded by the National Research Foundation of Korea (NRF) under grant 2021R1A2C1007044.

## References

- Ashley, W.S., Bentley, M.L., Stallins, J.A., 2012. Urban-induced thunderstorm modification in the Southeast United States. *Clim. Chang.* 113, 481–498.
- Baik, J.-J., Kim, Y.-H., Chun, H.-Y., 2001. Dry and moist convection forced by an urban heat island. *J. Appl. Meteorol.* 40, 1462–1475.
- Bornstein, R., LeRoy, M., 1990. Urban barrier effects on convective and frontal thunderstorms. Preprint. In: Conf. on Mesoscale Processes. Amer. Meteorol. Soc., Boulder, CO.
- Bornstein, R., Lin, Q., 2000. Urban heat islands and summertime convective thunderstorms in Atlanta: three case studies. *Atmos. Environ.* 34, 507–516.
- Braham Jr., R.R., 1979. Comments on “Urban, topographic and diurnal effects on rainfall in the St. Louis region”. *J. Appl. Meteorol.* 18, 371–375.
- Changnon Jr., S.A., 1979. Rainfall changes in summer caused by St. Louis. *Science* 205, 402–404.
- Changnon, S.A., Shealy, R.T., Scott, R.W., 1991. Precipitation changes in fall, winter, and spring caused by St. Louis. *J. Appl. Meteorol.* 30, 126–134.
- Daniels, E.E., Lenderink, G., Huitjes, R.W.A., Holtslag, A.A.M., 2016. Observed urban effects on precipitation along the Dutch west coast. *Int. J. Climatol.* 36, 2111–2119.
- Diem, J.E., Mote, T.L., 2005. Interepochal changes in summer precipitation in the southeastern United States: evidence of possible urban effects near Atlanta, Georgia. *J. Appl. Meteorol.* 44, 717–730.
- Doan, Q.-V., Dipankar, A., Simón-Moral, A., Sanchez, C., Prasanna, V., Roth, M., Huang, X.-Y., 2021. Urban-induced modifications to the diurnal cycle of rainfall over a tropical city. *Q. J. R. Meteorol. Soc.* 147, 1189–1201.
- Dou, J., Bornstein, R., Miao, S., Sun, J., Zhang, Y., 2020. Observation and simulation of a bifurcating thunderstorm over Beijing. *J. Appl. Meteorol. Climatol.* 59, 2129–2148.
- Dou, J., Wang, Y., Bornstein, R., Miao, S., 2015. Observed spatial characteristics of Beijing urban climate impacts on summer thunderstorms. *J. Appl. Meteorol. Climatol.* 54, 94–105.
- Fujibe, F., Togawa, H., Sakata, N., 2009. Long-term change and spatial anomaly of warm season afternoon precipitation in Tokyo. *SOLA* 5, 17–20.
- Haberlie, A.M., Ashley, W.S., Pingel, T.J., 2015. The effect of urbanisation on the climatology of thunderstorm initiation. *Q. J. R. Meteorol. Soc.* 141, 663–675.
- Han, J.-Y., Baik, J.-J., 2008. A theoretical and numerical study of urban heat island-induced circulation and convection. *J. Atmos. Sci.* 65, 1859–1877.
- Han, J.-Y., Baik, J.-J., Khain, A.P., 2012. A numerical study of urban aerosol impacts on clouds and precipitation. *J. Atmos. Sci.* 69, 504–520.
- Han, J.-Y., Baik, J.-J., Lee, H., 2014. Urban impacts on precipitation. *Asia-Pac. J. Atmos. Sci.* 50, 17–30.
- Hand, L.M., Shepherd, J.M., 2009. An investigation of warm-season spatial rainfall variability in Oklahoma City: possible linkages to urbanization and prevailing wind. *J. Appl. Meteorol. Climatol.* 48, 251–269.
- Hersbach, H., Bell, B., Berrisford, P., Hirahara, S., Horányi, A., Muñoz-Sabater, J., Nicolas, J., Peubey, C., Radu, R., Schepers, D., Simmons, A., Soci, C., Abdalla, S., Abellán, X., Balsamo, G., Bechtold, P., Biavati, G., Bidlot, J., Bonavita, M., Chiara, G.D., Dahlgren, P., Dee, D., Diamantakis, M., Dragani, R., Flemming, J., Forbes, R., Fuentes, M., Geer, A., Haimberger, L., Healy, S., Hogan, R.J., Hölm, E., Janíková, M., Keeley, S., Laloyaux, P., Lopez, P., Lupu, C., Radnoti, G., Rosnay, P.D., Rozum, I., Vamborg, F., Villaume, S., Thépaut, J.-N., 2020. The ERA5 global reanalysis. *Q. J. R. Meteorol. Soc.* 146, 1999–2049.
- Hjelmfelt, M.R., 1982. Numerical simulation of the effects of St. Louis on mesoscale boundary-layer airflow and vertical air motion simulations of urban vs non-urban effects. *J. Appl. Meteorol.* 21, 1239–1257.
- Huff, F.A., Changnon Jr., S.A., 1972. Climatological assessment of urban effects on precipitation at St. Louis. *J. Appl. Meteorol.* 11, 823–842.
- Jin, H.-G., Lee, H., Baik, J.-J., 2022. Characteristics and possible mechanisms of diurnal variation of summertime precipitation in South Korea. *Theor. Appl. Climatol.* 148, 551–568.
- Kim, Y.-H., Choi, D.-Y., Chang, D.-E., 2011. Characteristics of urban meteorology in Seoul metropolitan area of Korea. *Atmosphere* 21, 257–271 (in Korean with English abstract).
- Korean Statistical Information Service, 2021. Building Status by Number of Floors (accessed 31 December 2021). <https://kosis.kr>.
- Keuser, A.P.M., 2014. Precipitation patterns and trends in the metropolitan area of Milwaukee, Wisconsin. *Int. J. Geospat. Environ. Res.* 1, 6.
- Kug, J.-S., Ahn, M.-S., 2013. Impact of urbanization on recent temperature and precipitation trends in the Korean peninsula. *Asia-Pac. J. Atmos. Sci.* 49, 151–159.
- Kusaka, H., Nishi, A., Mizunari, M., Yokoyama, H., 2019. Urban impacts on the spatiotemporal pattern of short-duration convective precipitation in a coastal city adjacent to a mountain range. *Q. J. R. Meteorol. Soc.* 145, 2237–2254.
- Lee, S.-H., Baik, J.-J., 2010. Statistical and dynamical characteristics of the urban heat island intensity in Seoul. *Theor. Appl. Climatol.* 100, 227–237.
- Liu, J., Niyogi, D., 2019. Meta-analysis of urbanization impact on rainfall modification. *Sci. Rep.* 9, 7301.
- Lowry, W.P., 1998. Urban effects on precipitation amount. *Prog. Phys. Geogr.* 22, 477–520.
- Manola, I., Steeneveld, G.-J., Uijlenhoet, R., Holtslag, A.A.M., 2020. Analysis of urban rainfall from hourly to seasonal scales using high-resolution radar observations in the Netherlands. *Int. J. Climatol.* 40, 822–840.
- Ntelekos, A.A., Smith, J.A., Donner, L., Fast, J.D., Gustafson Jr., W.I., Chapman, E.G., Krajewski, W.F., 2009. The effects of aerosols on intense convective precipitation in the northeastern United States. *Q. J. R. Meteorol. Soc.* 135, 1367–1391.

- Ochoa, C.A., Quintanar, A.I., Raga, G.B., Baumgardner, D., 2015. Changes in intense precipitation events in Mexico City. *J. Hydrometeorol.* 16, 1804–1820.
- Oke, T.R., Mills, G., Christen, A., Voogt, J.A., 2017. Clouds and precipitation. In: *Urban Climates*. Cambridge University Press, pp. 270–293.
- Qian, Y., Chakraborty, T., Li, J., Li, D., He, C., Sarangi, C., Chen, F., Yang, X., Leung, R., 2022. Urbanization impact on regional climate and extreme weather: current understanding, uncertainties, and future research directions. *Adv. Atmos. Sci.* 39, 819–860.
- Rosenfeld, D., 2000. Suppression of rain and snow by urban and industrial air pollution. *Science* 287, 1793–1796.
- Schmid, P.E., Niyogi, D., 2017. Modeling urban precipitation modification by spatially heterogeneous aerosols. *J. Appl. Meteorol. Climatol.* 56, 2141–2153.
- Seino, N., Aoyagi, T., Tsuguti, H., 2018. Numerical simulation of urban impact on precipitation in Tokyo: how does urban temperature rise affect precipitation? *Urban Clim.* 23, 8–35.
- Shepherd, J.M., 2005. A review of current investigations of urban-induced rainfall and recommendations for the future. *Earth Interact.* 9, 1–27.
- Shepherd, J.M., Pierce, H., Negri, A.J., 2002. Rainfall modification by major urban areas: observations from spaceborne rain radar on the TRMM satellite. *J. Appl. Meteorol.* 41, 689–701.
- Suh, S.-H., You, C.-H., Lee, D.-I., 2016. Climatological characteristics of raindrop size distributions in Busan, Republic of Korea. *Hydrol. Earth Syst. Sci.* 20, 193–207.
- Takahashi, H., Nakamura, Y., Suzuki, H., 2011. Frequency distribution of intense rainfall in the wards of Tokyo and its relationship with the spatial structure of building heights. *J. Geogr.* 120, 359–381 (in Japanese with English abstract).
- United Nations, 2019. *World Urbanization Prospects: The 2018 Revision*. Population Division, Department of Economic and Social Affairs, United Nations.
- Vogel, J.L., Huff, F.A., 1978. Relation between the St. Louis urban precipitation anomaly and synoptic weather factors. *J. Appl. Meteorol.* 17, 1141–1152.
- Wu, M., Luo, Y., Chen, F., Wong, W.K., 2019. Observed link of extreme hourly precipitation changes to urbanization over coastal South China. *J. Appl. Meteorol. Climatol.* 58, 1799–1819.
- Yang, L., Tian, F., Smith, J.A., Hu, H., 2014. Urban signatures in the spatial clustering of summer heavy rainfall events over the Beijing metropolitan region. *J. Geophys. Res. Atmos.* 119, 1203–1217.
- Yang, P., Ren, G., Yan, P., 2017. Evidence for a strong association of short-duration intense rainfall with urbanization in the Beijing urban area. *J. Clim.* 30, 5851–5870.
- Yang, P., Ren, G., Yan, P., Deng, J., 2021. Urbanization reduces frequency of light rain: an example from Beijing city. *Theor. Appl. Climatol.* 145, 763–774.
- Yeo, M.J., Kim, Y.P., 2019. Trends of the PM<sub>10</sub> concentrations and high PM<sub>10</sub> concentration cases in Korea. *J. Korean Soc. Atmos. Environ.* 35, 249–264 (in Korean with English abstract).
- Yi, C., Kwon, T.H., Park, M.-S., Choi, Y.J., An, S.M., 2015. A study on the roughness length spatial distribution in relation to the Seoul building morphology. *Atmosphere* 25, 339–351 (in Korean with English abstract).